The 2015 World Congress on
Advances in Structural Engineering and Mechanics (ASEM15)
Incheon, Korea, August 25-29, 2015

Seismic assessment and base isolation of free-standing monumental marble columns

Camilla Bitossi[1)], Elena Mori[2)], Stefano Sorace[3)] and Gloria Terenzi[4)]

[1), 2), 4)] *Department of Civil and Environmental Engineering, University of Florence, Italy*
[3), 4)] *Department of Civil Engineering and Architecture, University of Udine, Italy*
[4)] *gloria.terenzi@unifi.it*

ABSTRACT

A new step of a research programme concerning the seismic performance assessment of art objects, and their enhanced protection by means of innovative base isolation solutions, is presented in this paper. Attention is particularly focused on free-standing monumental columns. Rocking and sliding effects are expressly modelled in the time-history analyses, so as to evaluate their influence beginning from the lowest normative seismic input levels. The case study marble column examined here exhibits a rocking-affected response for the action scaled at the basic design earthquake, and potential overturning-induced collapse under seismic action scaled at the maximum considered earthquake level. The response becomes safe and undamaged thanks to the proposed retrofit intervention, which consists in base-isolating the bearing floor of the location where the column is situated.

1. INTRODUCTION

Moderate-to-severe earthquakes cause serious damages to various types of contents, in addition to structures and infrastructures. Art objects are among the most vulnerable assets, as a consequence of their intrinsic weakness, limited mechanical redundancy and, in most cases, free-contact installations with the interfacing surfaces (floors, walls, etc). The peculiar dynamic behaviour of the artefacts, which includes sliding and rocking effects in case of unanchored connections, can cause the objects to lose equilibrium, and thus overturn and fall off. In view of this, the response of exhibits has been traditionally analysed within the context of the dynamics of rigid blocks (Yim et al. 1980, Ishiyama 1982, Shenton and Jones 1991, Caliò and Marletta 2003). Based on the computation of the position of the center of gravity of an object or object assembly, simple relations can help quickly assess rocking and overturning conditions and the maximum seismic action for which these are not reached. Therefore, they

[1), 2)] Engineer
[3), 4)] Professor

implicitly focus on the basic performance level (PL) represented by Collapse prevention.

The modelling possibilities now offered by finite element methods allow extending the seismic analysis of art objects to under-critical response levels, with the aim of carrying out thorough performance assessment enquiries. The following set of limit states was recently formulated to this aim (Sorace and Terenzi 2015): 1) Rest; 2) No rocking; 3) Damage control; and 4) the above-mentioned basic PL of Collapse prevention.

The first level corresponds to the transmission of purely compressive normal stresses from the base of the object to the floor. Rest conditions terminate when the first decompression of a joint belonging to the base section is reached. Although not coinciding with the attainment of rocking, this configuration can determine non negligible local amplifications of the response parameters, and thus it must be checked properly. The boundary of level 2) corresponds to the onset of rocking, which is identified by repeated uplifts of appreciable amplitude of sets of joints belonging to opposite sides of the base section. The upper limit of level 3) is assumed to coincide with the appearance of visible cracks, for elements made of materials with small tensile strength (i.e. whose tensile strength is lower than 1/10 of the compressive strength), or local plasticizations, for metallic artworks. These represent limit conditions for the safeguard of the artistic value of the objects too. Therefore, the performance level of Damage control can also be labelled as “Artistic value safety”. The limit conditions of level 4) are represented by the achievement of overturning-induced loss of stability, in case of slender objects, or structural collapse, for massive and squat elements. The former condition is normally not highlighted in output by the finite element analysis, and thus it must be deducted from additional evaluations, as discussed in Section 3 below. Collapse is directly identified by the divergence of the numerical solution, for non-linear cracking or plastic models, whereas it must be characterised by approximate criteria, like for the loss in stability, when elastic models are adopted.

A study concerning slender free-standing artworks is presented in this paper, with the aim of extending to this class of objects a research dedicated to the evaluation of seismic vulnerability and the advanced protection of exhibits, initially focused on massive statues made of small tensile strength materials (Sorace and Terenzi 2015). A demonstrative example, represented by a marble column to be temporarily placed, for the development of restoration works, in the Laboratories of Stones and Bronzes of the world-famous Opificio delle Pietre Dure Institute in Florence, is examined. The criteria followed to carry out the multi-level performance assessment analysis, and a synthesis of relevant results, are reported. A special seismic isolation retrofit intervention, which consists in incorporating the protective system at the base of the bearing floor of the Laboratories, is then proposed. Technical and modelling details of the adopted isolators are offered, and the benefits reached in the performance of the case study column thanks to the rehabilitation solution are discussed.

2. CASE STUDY COLUMN

The ground floor plan of the Opificio delle Pietre Dure Institute is shown in Fig. 1, where the L-shaped wing of the Laboratories of Stones and Bronzes is highlighted by a hatched background and a continuous-line perimeter contour.

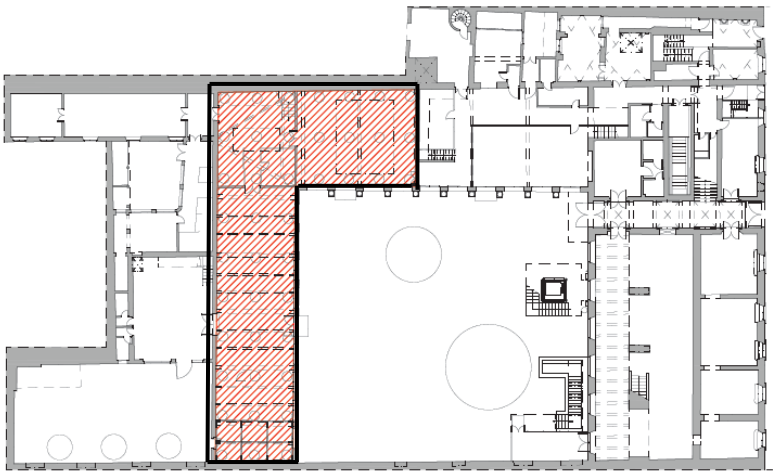

Fig. 1 Plan of the ground floor of Opificio delle Pietre Dure Institute in Florence, with the Laboratories of Stones and Bronzes wing highlighted by a hatched background

The case study column is a sculpted monobloc marble element shaped as a semicircular drum, with a multilayer toroidal ring at the bottom and no capital on top, and a parallelepiped basement, as illustrated in the drawing of Fig. 2. The dimensions of the basement in plan are A=724 mm × B=450 mm. The heights of basement, multilayer ring and drum are 750 mm, 312 mm and 2085 mm, respectively, for a total height H of 3147 mm. A simulated view of the installation of column in the area of the Laboratories where the restoration works will be carried out is shown in Fig. 3.

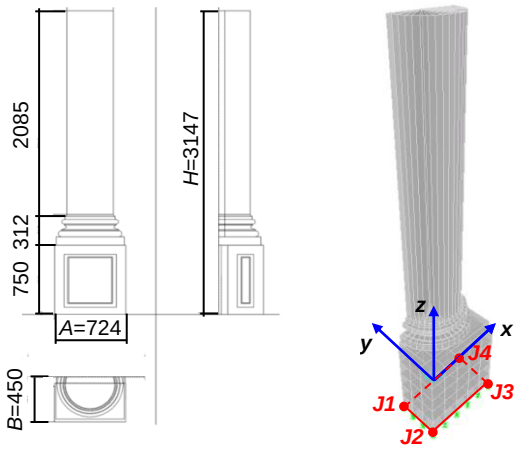

Fig. 2 Prospects (dimensions in millimeters) of the case study column, and view of the finite element model used in the analyses

The constituting material is cipolin marble, traditionally used for ornamental elements, such as floors, coverings, cornices, balustrades and standing alone columns, like the examined one, rather than as main construction material for structural systems. As no characterization tests were carried out on the material, its mechanical properties were established by referring to the following typical ranges of variation suggested for

this type of marble in the literature (Malesani and Vannucci 1974, Scesi et al. 2006): uniaxial compressive strength f_c=40–60 MPa; uniaxial tensile strength f_t=0.5–0.8 MPa; Young modulus E=20,000–40,000 MPa; Poisson coefficient ν=0.28–0.32; specific weight γ=25–27 kN/m^3. In consideration of the absence of direct diagnostic tests, as well as of the ageing and creep-related strength decay occurring throughout the structural life of marbles and stones (Sorace 1996), the lowest values of the strength ranges above, i.e. f_c=40 MPa and f_t=0.5 MPa, were assumed as a reference in the analysis. Concerning E, ν and γ, the average values of relevant ranges, E=30,000 MPa, ν=0.3 and γ=26 kN/m^3, were adopted throughout the numerical enquiry.

Fig. 3 Photomontage view of the column in the Laboratories of Stones and Bronzes

Unlike the geometrically complex case study marble statue examined in (Sorace and Terenzi 2015), where a smeared-crack numerical model was adopted to carefully detect the evolution of cracking-related damage in the most stressed portions of the mesh, the analysis here was limited to the elastic field for the examined column, in consideration of its very simple shape and structural configuration. Indeed, these characteristics allow easily locating at the base of the drum the most critical zones where crack can arise and grow. The onset of cracks is identified by comparing the maximum computed tensile stress values with f_t. A 3-D view of the finite element model, generated by SAP2000NL commercial software (CSI 2014), and the reference global coordinate system, are displayed in Fig. 2 too. The mesh is made of 8-node isoparametric solid-type elements, with parallelepiped shape, for the basement, and prismatic shape, for the drum and the bottom ring. Rocking is simulated by means of a set of vertical “gap” (no-tension) interface elements, linking the joints of the base section of the basement to the ground. Sliding is simulated by plan horizontal friction sliders linking the same joints as the gap elements. Based on literature suggestions (Gordon 1976, ASTM 2011), the sliding friction coefficient between marble and the cotto-tile surface constituting the floor was fixed at 0.3.

3. PERFORMANCE ASSESSMENT ANALYSIS IN CURRENT CONDITIONS

A modal analysis of the column was preliminarily carried out, which highlighted a first vibration mode purely translational along y, with period of 0.153 s and effective modal mass equal to 34% of the total seismic mass. The second mode is mixed

translational along *x*–rotational around *z*, with period of 0.086 s and masses of 35%, along *x*, and 6%, around *z*. Six modes are needed to activate summed modal masses nearly equal to 90% along all three axes.

The seismic performance evaluation enquiry was carried out for the four reference earthquake levels established by current Italian Standards (Italian Council of Public Works 2008), that is, Frequent Design Earthquake (FDE, with 81% probability of being exceeded over the reference time period V_R); Serviceability Design Earthquake (SDE, with 50%/V_R probability); Basic Design Earthquake (BDE, with 10%/V_R probability); and Maximum Considered Earthquake (MCE, with 5%/V_R probability). The V_R period is fixed at 50 years, which is obtained by multiplying the nominal structural life V_N of 50 years by a coefficient of use c_u equal to 1. The latter value is adopted because the Laboratories is a one-storey wing with staff-only reserved access (i.e. not subject to heavy afflux of visitors), separated from the main three-storey wing of the building, where the state museum of the Institute, open to the public, is housed. By referring to topographic category (TC) equal to T1 (flat surface), and C-type soil (deep deposits of dense or medium-dense sand, gravel or stiff clay from several ten to several hundred meters thick), the peak ground accelerations for the four seismic levels are as follows: 0.071 *g* (FDE), 0.085 *g* (SDE), 0.197 *g* (BDE), and 0.244 *g* (MCE), with *g*=acceleration of gravity.

The input accelerograms were generated by SIMQKE-II software (Vanmarcke et al. 1999) in families of seven, both for the horizontal and vertical components of seismic action, from the pseudo-acceleration response spectra at linear viscous damping ratio ξ=5% prescribed by the Italian Standards for Florence city, plotted in Fig. 4. As required by the same Standards, as well as by Eurocode 8 (2004) and several other international seismic regulations, in each time-history analysis the accelerograms were applied in groups of three simultaneous components, i.e. two horizontal components, with the first one selected from the first generated family of seven motions, and the second one selected from the second family, plus the vertical component.

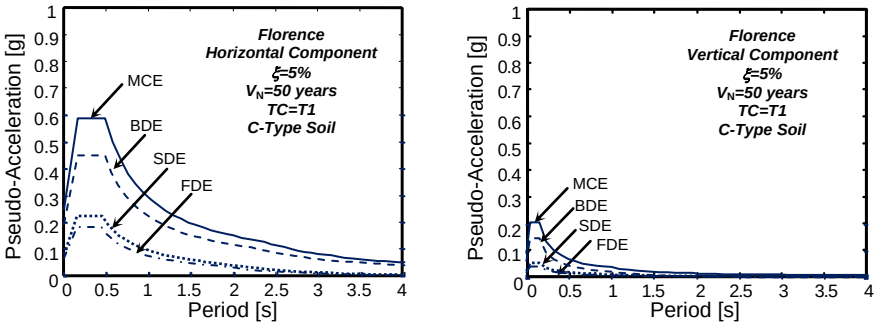

Fig. 4 Normative pseudo-acceleration elastic response spectra for the horizontal and vertical earthquake components – Florence city. FDE, SDE, BDE and MCE levels

In order to assess the seismic performance of the case study column, as well as of any free-standing art object, the limit conditions of Rest and Damage control/Artistic value safety PLs can be directly deducted from the results of the time-history analyses. Indeed, as observed in the Introduction, they correspond to: the first decompression of

at least a joint belonging to the base section, caused by the most unfavourable combination of the effects of the three earthquake components in proximity to a section edge — Rest; and the attainment of the tensile strength f_t in the portions of the mesh subjected to the highest tensile stress values — Damage control, respectively. Both conditions are easily detectable in the post-processing stage.

On the other hand, quantitative criteria are needed to identify the boundaries of No rocking and Collapse prevention PLs. Concerning the former, the necessary physical condition for a vertical oscillation of the base section of the object, considered as a rigid body, around a perimeter side is reached when the seismically induced moment determined by the resultant of the horizontal inertia forces applied in center of mass G, M_s, equals the available resisting moment due to gravity, M_r, with M_s and M_r computed with respect to this side. The "critical" response acceleration a_c causing this condition is

$$a_c = \frac{b_G}{h_G} \cdot g \tag{1}$$

where b_G is the distance of the vertical projection of G from the nearest side of the base section in plan, which represents the axis of rotation (relative to the ground) for the considered oscillation plan, and h_G is the height of G from the base section. The values of b_G and h_G are highlighted in Fig. 5 for the main oscillation plan of the column (y-z, x being the weak flexural axis), where M_s and M_r are symbolically indicated too. By applying (1) for b_G=150 mm and h_G=1190 mm, a_c=0.126 g is obtained.

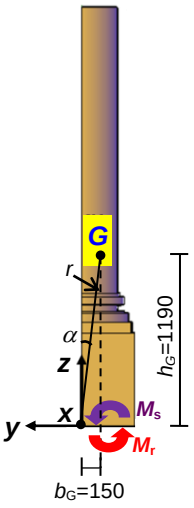

Fig. 5 Coordinates of the center of mass and reference symbols for the analysis

It should be noted that the a_c estimate provided by (1), in addition to the assumed rigid body hypothesis, also neglects the effects of the upward earthquake component, as well as of the interaction of rocking with sliding. Therefore, the a_c value is only a first-level approximation in the assessment analysis, constituting a useful comparative term for the time-history finite element results. In order to identify an actual rocking dynamic

response regime from latter, the minimum number of uplifts of two opposite sides in plan, n_u, and their amplitude, d_v, must be preliminary fixed. Based on the results of computational studies carried out at a first stage of this research on several types of artworks, including slender objects, the following values were suggested (Sorace and Terenzi 2015): five, for n_u, and 0.5 mm, for d_v. In particular, the d_v limit represents a threshold beyond which rocking-related uplifts proved to be substantially unaffected by the numerical accuracy of the finite element non-linear solution, which are related to the time-integration step choice, the elastic compression stiffness of the vertical gap elements, the solid element mesh dimensions (and thus the number of gaps linking the base section to the substrate), as well as by the interaction with sliding. At the same time, n_u=5 is a minimal value separating an alternate rocking regime of uplifts from sporadic detachments from the ground with amplitude greater than d_v, independently from the specific characteristics of the input ground motions (whether of near or far-fault type, natural or artificially generated, amplitude-scaled or not, etc). The n_u and d_v values above were assumed as a reference also for the analysis of the case study column.

As regards the limit conditions of Collapse prevention level, supplementary criteria must be adopted to identify the overturning-related collapse limit condition. In the rigid-body hypothesis, the classical mixed acceleration–velocity criterion proposed by Ishiyama (1982) can be assumed, for which the lower acceleration limit is given by the rocking relation (1), whereas the lower velocity capable of overturning the rocking body, v_c, is approximately expressed as follows:

$$v_c = 0.4\sqrt{\frac{2g}{r}\left(i^2 + r^2\right)\frac{1-\cos\alpha}{\cos^2\alpha}} \tag{2}$$

where i is the radius of gyration of the body about G, r is the distance from the base edge to G, and α is the angle between the vertical axis z and the segment joining the base edge to G ($\alpha = \text{arctg}\left(\frac{b_G}{h_G}\right)$), in rest conditions, as shown in Fig. 5 scheme too. For a rectangular body, $i^2 + r^2 = \frac{4}{3}r^2$, in which case equation (2) becomes:

$$v_c = 0.4\sqrt{\frac{8gr}{3}\frac{1-\cos\alpha}{\cos^2\alpha}} \tag{3}$$

In order to apply (3) when the body is not rectangular and also non-symmetric in the main oscillation plan, but is divided in geometrically regular portions and thus the position of the center of mass can be precisely calculated, it can be idealized as an equivalent rectangular block with base equal to $2b_G$. This schematization was numerically validated by Boroschek and Romo (2004) for a wide variety of non-symmetrical bodies, as well as of input ground motions, and further checked on

experimental basis by Boroschek and Iruretagoyena (2006).

The results of the computational analyses are synthesised in Figs. 6 and 7. The vertical displacement histories obtained from the most demanding among the seven groups of input accelerograms are plotted in Fig. 6 for the four normative earthquake levels. The graphs are referred to the edge joints of the most distant side of the base section from the vertical projection of *G*, denoted with symbols *J2* and *J3* in the finite element model view of Fig. 2.

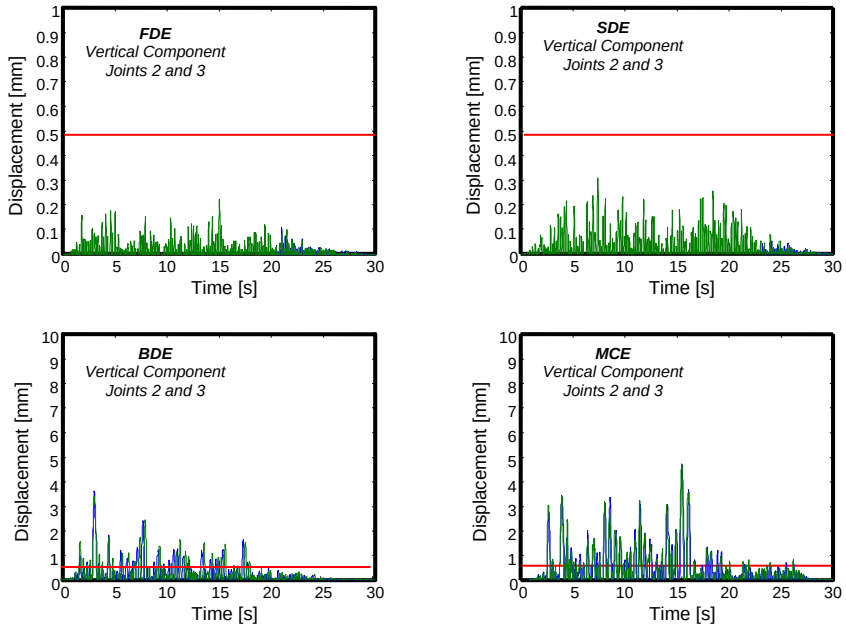

Fig. 6 Vertical displacement time-histories of joints *J2* and *J3*

The graphs show several small uplifts for the FDE and BDE-scaled actions, with peak values slightly greater than 0.2 mm (FDE) and 0.3 mm (SDE), both neatly below the 0.5 mm threshold, highlighted by a red segment in these diagrams. This response corresponds to the decompression of a portion of the base section, assessing that the Rest performance level is exceeded, and the response consequently falls in the No rocking range. These data corroborate the first-level evaluation based on the comparison of a_c with the above-mentioned peak ground accelerations for the FDE and SDE, equal to 0.071 *g* and 0.085 *g*. Both values are lower than a_c, practically in the same proportion between the peak uplifts and the 0.5 mm limit, thus prefiguring the No rocking response conditions confirmed by the results of the time-history analyses.

The maximum vertical displacements reach 3.7 mm and 4.8 mm at the BDE and MCE, respectively, which are about 7 and 9 times greater than the assumed rocking threshold, which is repeatedly exceeded during the response. The peak values of the time-history uplifts of the edge joints of the opposite side in plan (*J1*, *J4* according to the nomenclature in Fig. 2), not presented here for brevity's sake, are about half the values found for *J2*, *J3*. This fraction is well correlated with the ratio of the distances of the two sides from the vertical projection of *G*, $b_G/(B-b_G)=150/(300-150)=0.5$.

In order to evaluate whether the activation of this pronounced rocking regime also

corresponds to the attainment of the Damage Control limits, the vertical tensile stress distributions obtained at the BDE and MCE for the same groups of input accelerograms which the two lower graphs in Fig. 6 are referred to, are reproduced in Fig. 7.

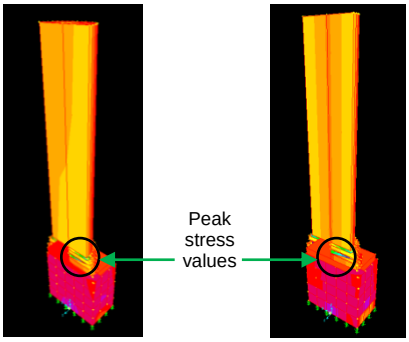

Fig. 7 Vertical tensile stress contours for the BDE (left) and MDE

As expected, the most stressed portion of the mesh is situated across the multi-layer ring zone at the base of the drum, marked with circles in the finite element model views of Fig. 7. The peak stress values, surveyed in the rear side of the second ring from the bottom, characterised by the smallest cross section, are equal to 0.58 MPa (BDE) and 0.77 MPa (MCE), i.e. about 15% and 50% greater than f_t. This underlines that cracks might already open in this ring at the BDE, thus exceeding the limit conditions of Damage control/Cultural value safety PL, and significantly spread to the other rings and the base section of the drum at the MCE.

The possible overturning of the column is checked by means of expression (3), which provides the following critical velocity for the equivalent base width, $2b_G$=300 mm, in the *y*-*z* plan: v_c=202 mm/s, being i=1199.5 mm and α=7.18°. By comparing v_c with the peak ground velocity for the BDE and MCE, equal to 145.6 mm/s and 183.8 mm/s, respectively, near-overturning conditions are assessed for the highest earthquake level. Indeed, the difference between the MCE-related peak velocity and v_c, lower than 10%, represents a small safety margin, in consideration of the inherent approximations involved in v_c calculation.

By summing up the results of the performance assessment analysis, in addition to the FDE–No rocking and SDE–No rocking correlations commented above, BDE–Collapse prevention and MCE–Collapse prevention correlations are found, with small overturning collapse-related safety margins for the MCE.

Additional information on the column performance is derived from the sliding response. As highlighted by the horizontal displacement time-histories of the base section computed for the BDE and MCE, plotted in Fig. 8 for the most demanding groups of input motions and *J2*, *J3* joints too, peaks of 4 mm (BDE) and 6 mm (MCE) are obtained. These values are high enough to cause possible pounding conditions should the column be leaning against other artworks or a wall during the restoration works, instead of at the center of the Laboratories. Furthermore, the response histories of the two joints notably differ at both earthquake levels, and are also divergent at the MCE, highlighting remarkable torsional effects due to asymmetry of the column in the *y*-

z plan, as well as to the combined action of the earthquake components along axes *x* and *y*.

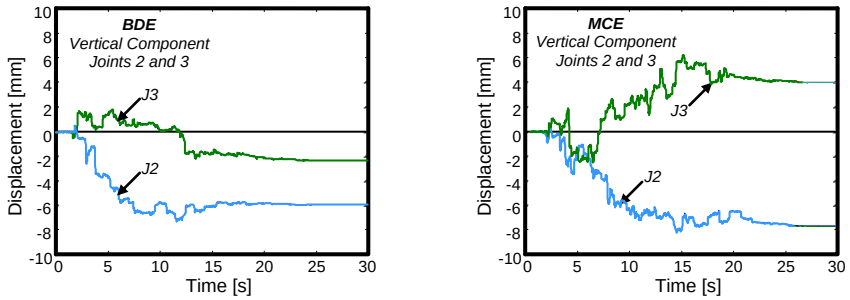

Fig. 8 Horizontal displacement time-histories of joints *J2* and *J3*

4. BASE ISOLATION RETROFIT HYPOTHESIS

The retrofit hypothesis proposed for the Laboratories floor consists in incorporating a set of 42 isolators, constituted by double curved surface slider (DCSS) elements with equal sliding spherical surfaces, on top of a correspondingly equal number of supporting reinforced concrete (R/C) columns. The columns are built in a volume obtained by demolishing the existing cotto-tile floor (a modern finish of no historical or artistic value) and the underlying loose stone layer, and by digging about 2.5 m deep in the ground. The resulting basement area will also enable easy inspection, maintenance, and removal (for future testing or replacement) of the DCSS devices. The new floor is made of 55 mm-high HI-bond corrugated steel sheets with a 50 mm-thick on-site cast R/C slab on top, aimed at obtaining a horizontal rigid diaphragm effect for the isolation plan. The main structure consists of primary and secondary beams in HEA 160 and HEA 100 Italian profiles, respectively, made of S235JR grade steel.

A cross section, photographic view and schematic total reaction force–displacement [F_t–d] response cycle of a DCSS isolator are shown in Fig. 9. F_t is given by the sum of the pendulum response component, F_p, relevant to the isolation function of the device, and the friction component, F_f, governing its dissipative function. The time-dependent expressions of F_p, F_f and F_t are as follows (Fenz and Constantinou 2006, Sorace and Terenzi 2014):

$$F_p(t) = \frac{W(t)}{L_{DCSS}} d(t) \tag{4}$$

$$F_f(t) = \mu W(t) \tag{5}$$

$$F_t(t) = \frac{W(t)}{L_{DCSS}} d(t) + \mu W(t) \tag{6}$$

where $V(t)$=vertical load, L_{DCSS}=effective double pendulum length, and μ=friction coefficient of the lubricated thermoplastic sliding surfaces.

Fig. 9 Cross section, view and schematic response cycle of a DCSS isolator with equal sliding surfaces

The equivalent vibration period of the isolator, T_e, associated to the linear equivalent (or secant) stiffness of the isolator, k_e, shown in the cycle of Fig. 9 is

$$T_e = 2\pi \sqrt{\frac{1}{g\left(\frac{1}{L_{DCSS}} + \frac{\mu}{d_{max}}\right)}} \tag{7}$$

with d_{max}=maximum displacement of the device. The actual vibration period of the isolator in dynamic response conditions, T_d, associated to the "restoring" (or tangent) stiffness, k_r, also highlighted in the reference cycle of Fig. 9, is

$$T_d = 2\pi \sqrt{\frac{L_{DCSS}}{g}} \tag{8}$$

Based on a preliminary sizing carried out by estimating the maximum displacement demand for the MCE seismic level, the following values of L_{DCSS}, μ and d_{max} parameters included in relations (4) through (8) were selected, as derived from the reference manufacturer's catalogue (FIP 2014): L_{DCSS}=2535 mm; μ=0.025; d_{max}=±200 mm; $T_e(d_{max})$=2.78 s; and T_d=3.18 s. The remaining mechanical and geometrical properties are: $\xi_e(d_{max})$= equivalent linear viscous coefficient at the maximum displacement=15.3%; D=diameter=400 mm; and H=height=84 mm.

The finite element model of the DCSS isolators was generated by the "Friction isolator" link available in the library of SAP2000NL software, which allows exactly reproducing the behaviour described by expressions (4) through (8). The link, also used as plan slider element to simulate the sliding effects of the column, was modelled with curved surfaces geometrically defined by the L_{DCSS} and D values above. A view of the of the mesh of the mobile floor, composed of frame-type elements and incorporating at the 42 links by which the DCSS isolators are schematised, is displayed in Fig. 10.

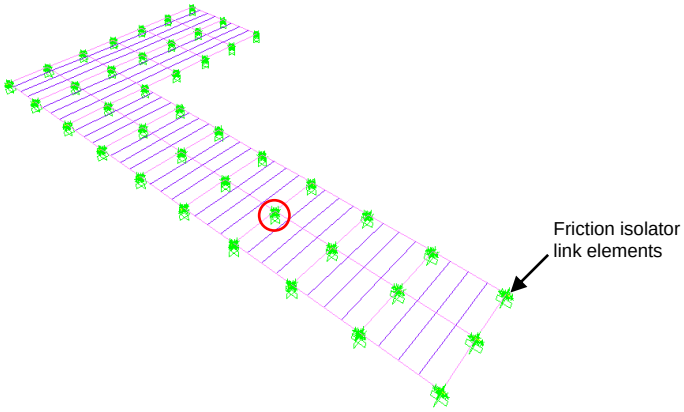

Fig. 10 Finite element model of the isolated floor

The results of the time-history verification analyses in base-isolated conditions show null uplifts and practically null sliding displacements for the input actions scaled up to the MCE level. These data correspond to the attainment of Rest PL for all four earthquake levels, in terms of dynamic performance. In order to check the corresponding stress demand, the contour maps of the vertical normal values are reproduced in Fig. 11 for the most demanding motions scaled at the MCE. The peaks of these distributions are located in the same critical portions of the mesh as identified in fixed-base floor configuration, but reduced to 0.13 MPa, i.e. only ¼ f_t, which brings evidence of totally undamaged response up to the highest earthquake level. By comparing these values with the corresponding maximum values computed in current conditions, a drop of about 85% is obtained at the MCE thanks to the filtering action of the isolation system. Furthermore, the MCE-related peaks surveyed after retrofit are remarkably lower than the maximum stresses obtained for the fixed-base floor even at the FDE level.

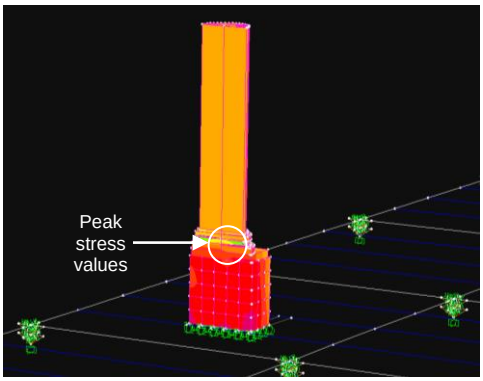

Fig. 11 Vertical tensile stress contour for the MDE in base-isolated floor conditions

Concerning the isolation system performance, it is illustrated by the [F_t–d] response cycles of the DCSS slider highlighted with a circle in Fig. 10, plotted in Fig. 12 for the x and y axes of the coordinate system assumed to generate the floor mesh,

coinciding with the *x* and *y* axes adopted for the column. It is noted that similar peak displacements are surveyed for all remaining devices, as a consequence of the small influence of the plan torsional component on the response of the mobile floor. A maximum displacement value of about 95 mm is recorded for all isolators, which is slightly lower than 50% of the isolator displacement capacity d_{max}, thanks to the supplemental damping action of the protective system supplied by the frictional capacity of the DCSS devices.

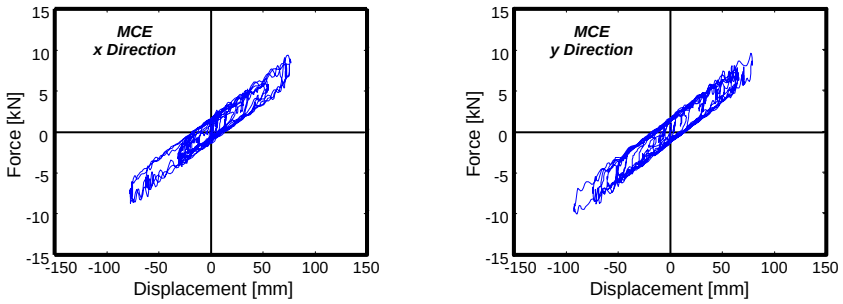

Fig. 12 Response cycles at the MCE of the DCSS isolator highlighted in Fig. 10

5. CONCLUSIONS

The new step of a research programme dedicated to the evaluation of the seismic performance of art objects confirmed for the stand-alone marble column examined here, i.e. a representative case study of slender artworks in free contact with the bearing floor, a high vulnerability also when such objects are situated in moderate seismicity sites, like Florence.

Indeed, relatively low performance was assessed in current conditions by the finite element time-history verification analyses, synthesized by the FDE–No rocking, SDE–No rocking, BDE–Collapse prevention and MCE–Collapse prevention correlations between earthquake and performance levels.

The base-isolation retrofit strategy proposed for the bearing floor of the Laboratories where the column will be located, along with several other art objects under restoration, allows reaching fully protected response conditions, as assessed by the attainment of Rest performance level up to the MCE. Furthermore, the maximum tensile stress values obtained at the MCE are lower than the corresponding peaks computed even at the FDE in current conditions.

The intervention is respectful of the architectural value of the Laboratories, as it is limited to the demolition of a modern standard floor of no artistic significance, and at the same time, it does not interfere with the elevation masonry structure of the building.

ACKNOWLEDGEMENTS

The study reported in this paper was sponsored by the Italian Department of Civil Protection within the ReLUIS-DPC Project 2014/2016. The authors gratefully acknowledge this financial support.

REFERENCES

ASTM (2011), *D2047-11. Standard Test Method for Static Coefficient of Friction of Polish-Coated Flooring Surfaces as Measured by the James Machine*, ASTM International, West Conshohocken, PA, 2011.

Boroschek, R. and Romo, D. (2004), "Overturning criteria for non-anchored non-symmetric rigid bodies," 13th World Conference on Earthquake Engineering, Vancouver, Canada, 2004, Paper No. 295.

Boroschek, R. and Iruretagoyena, A. (2006), "Controlled overturning of unanchored rigid bodies," *Earthquake Engineering and Structural Dynamics*, **35**, 695-711.

Caliò, I. and Marletta, M. (2003), "Passive control of the seismic rocking response of art objects," *Engineering Structures*, **25**, 1009-1018.

CSI (2014), *SAP2000NL. Structural analysis programs – Theoretical and users' manual*, Release no. 16.10, Berkeley, CA.

Eurocode 8 (2004), *Design of structures for earthquake resistance. Part 1: General rules, seismic actions and rules for buildings*, European Commission, Bruxelles, Belgium.

Fenz, D.M. and Constantinou, M.C. (2006), "Behaviour of the double concave friction pendulum bearing," *Earthquake Engineering and Structural Dynamics*, **35**, 1403-1424.

FIP (2015), *Anti-seismic devices product division*, http://www.fip-group.it.

Gordon, J.E. (1976), *The Science of structures and materials*, Scientific American Library, New York, NY.

Ishiyama, Y. (1982), "Motion of rigid bodies and criteria for overturning by earthquake excitations," *Earthquake Engineering and Structural Dynamics*, **10**, 630-650.

Italian Council of Public Works (2008), *Technical Standards on Constructions* [in Italian], G.U., Rome, Italy.

Malesani, P.P. and Vannucci, S.A. (1974), *Research on degradation of stones*, Leo Olschky, Florence, Italy.

Scesi, L., Papini, M. and Gattinoni, P. (2006), *Geologia applicata: il rilevamento geologico tecnico* [in Italian], Editrice Ambrosiana, Milan, Italy.

Shenton, H.W. and Jones, N.P. (1991), "Base excitation of rigid bodies. I: Formulation," *Journal of Engineering Mechanics, ASCE*, **117**, 2286–2306.

Sorace, S. (1996), "Creep in building stones under tensile conditions," *Journal of Engineering Materials and Technology, ASME*, **118**, 461-467.

Sorace, S. and Terenzi. G. (2014), "Motion control-based seismic retrofit solutions for a R/C school building designed with earlier Technical Standards," *Bulletin of Earthquake Engineering*, **12**, 2723-2744.

Sorace, S. and Terenzi, G. (2015), "Seismic performance assessment and base isolated floor-protection of statues exhibited in museum halls," *Bulletin of Earthquake Engineering*, **13**, 1873-1892.

Vanmarcke, E.H., Fenton G.A. and Heredia-Zavoni E. (1999), *SIMQKE-II. Conditioned earthquake ground motion simulator: User's manual*, Princeton University, Princeton, NJ.

Yim, C.S., Chopra, A. and Penzien, J. (1980), "Rocking response of rigid blocks to earthquakes," *Earthquake Engineering and Structural Dynamics*, **8**, 565-587.